Multiconfiguration linear-response approaches to the calculation of absolute photoionization cross sections: HF, H_2O, and Ne

H. Ågren

Institute of Physics and Measurement Technology, University of Linköping, S-58183, Linköping, Sweden

V. Carravetta

*Istituto di Chimica Quantistica ed Energetica Molecolare del Consiglio Nazionale delle Ricerche,
Via Risorgimento 35, 56100 Pisa, Italy*

H. J. Aa. Jensen

Department of Chemistry, University of Odense, DK-5230 Odense M, Denmark

P. Jørgensen

Department of Chemistry, University of Aarhus, DK-8000 Aarhus, Denmark

J. Olsen

Department of Theoretical Chemistry, Chemical Centre, Box 714, S-22007, Lund, Sweden

We describe multiconfiguration linear-response (MCLR) approaches to the calculation of absolute photoionization cross sections. Three algorithms are described: (i) one in which the MCLR equations are used to derive the primitive spectrum of excitation energies and oscillator strengths; (ii) one in which the solutions of the MCLR equations are used to provide the even negative moments of the photoexcitation-photoionization spectrum; and (iii) one in which a pseudospectrum is obtained directly in the iterative procedure used to solve the MCLR equations. Either the primitive spectra (i), the moments (ii), or the pseudospectra (iii) are used as basic quantities in Stieltjes imaging to obtain the photoionization cross sections. Numerical demonstrations with large multiconfigurational self-consistent field reference spaces are given for the photoionization of HF, H_2O, and Ne. Comparative calculations are performed in the random-phase approximation. Results are analyzed with respect to the fulfillment of gauge invariance, sum rules, basis-set completeness, and choice of correlating orbital spaces. Results for absolute photoionization cross sections from the MCLR algorithms agree very well with Stieltjes-imaging cross sections obtained from the semiempirically determined spectral moments of Meath and co-workers [Can. J. Phys. **55**, 2080 (1977); **63**, 1616 (1985)], and distinguish the raw experimental cross sections.

PACS number(s): 33.80.Eh

I. INTRODUCTION

The dynamics of photoionization processes have long been of considerable interest for experimental and theoretical studies. By means of energy and polarization variable excitation sources various resonant phenomena in continuum spectra of atoms and small molecules have been discovered and analyzed. More recent experimental studies focus on spectroscopy of surface adsorbate molecules for which resonances and other spectral features are interpreted in terms of surface bond strength and orientation of the adsorbate [3].

A problem in the theoretical description of photoionization resonances lies in the treatment of the scattering states due to the construction of the explicit continuum electronic wave functions in nonisotropic potentials. Conventional scattering approaches relying on asymptotic boundary conditions have met considerable difficulties in solving this problem, while so-called L^2 methods have an inherent potential in this respect due to the utilization of square-integrable basis sets to describe the noncentral character of the bound and continuum functions. In the L^2 approaches the many-electron continuum is generally approximated by an antisymmetrized product of a fixed target function for the molecular ion and a continuum orbital for the outgoing electron, the so-called static exchange approximation. Out of the L^2 methods mainly three branches have been developed: moment-theory approaches [4,5], K-matrix approaches [6,7], and complex-basis approaches [8,9].

An appealing feature of the moment-theory approaches is that they provide a direct generalization of the bound-state electronic structure methods and even the very computer codes, with the distinct advantage that both discrete and continuum states can be treated on a common basis, using the same point-group symmetry, integral representations of operators, etc. The correct energy normalization of the continuous part of the spectra is obtained from pointwise convergence of the spectral density. The formal motivation for the moment methods originates from the fact that, although the solutions of the Schrödinger equation in a square-integrable basis set

are proper representations only for the discrete part of the spectrum, they provide proper representations of the *moments* of the spectrum.

In the Stieltjes imaging approach, originally developed by Langhoff [4,5], a primitive Schrödinger spectrum of order N is converted to a spectrum (quadrature spectrum) of order n ($n \ll N$) such that the first $2n$ moments of the spectrum are reproduced. This quadrature spectrum is then used to form the Stieltjes derivative of the integral oscillator strength distribution that is proportional to the correctly energy-normalized cross section. The primitive spectrum has been generated with different techniques, in particular improved virtual-orbital (IVO) [10] and Lanczos techniques [11] corresponding to the static exchange approximation for single-channel and multichannel calculations. Common to these approaches is that the photoelectron function is assumed strongly orthogonal to a fixed target function, and that polarization and correlation of the latter with the photoelectron is not accounted for. This approach is well justified for high excitation energies, for which the sudden approximation applies, but may become more doubtful for slowly escaping photoelectrons at threshold or at low-lying shape resonances.

The use of linear-response (LR) methods, or polarization propagators, in connection with moment-theory calculations of photoionization cross sections has been proposed and investigated by Cacelli, Carravetta, and Moccia [7,12,13], Swanström *et al.* [14], and Müller-Plathe and Diercksen [15]. The basically applied low-order method is the random-phase approximation (RPA); however, the latter authors also exploited the multiconfigurational time-dependent Hartree-Fock (MCTDHF) [14] and the second-order polarization-propagator approximation (SOPPA) [15] methods. With the recent implementation [16] of multiconfigurational linear-response (MCLR) [17] approaches for large-scale reference wave functions [18] it has been possible to obtain excitation spectra for very accurate reference wave functions. This has been demonstrated in our recent application of MCLR to the calculations of excitation energies and Stieltjes imaging of the photodetachment cross sections of the notoriously difficult Li^- system [19]. It was shown that with a full variational form of the wave function only small expansions in terms of configurational and orbital parameters are needed to describe the exotic electronic structure and to obtain the shape resonance and the polarizability very accurately.

In the present work we describe how the solutions of the multiconfigurational linear-response equations can be used also to describe continuum- (shape-) resonant phenomena beyond the ionization threshold. With the MCLR approaches a description of the photoionization dynamics is obtained that also accounts for correlation (or polarization) of the residual ion to the photoelectron, and which thus goes beyond the strong orthogonality condition imposed in static exchange approximations. The MCLR equations are solved for the primitive spectrum of excitation energies and oscillator strengths as utilized in the previous application on Li^- [19]. In the present work we also propose an algorithm for solving MCLR equations that provides the even negative mo-

ments of a photoexcitation-photoionization spectrum directly. We also show how a pseudospectrum is obtained directly in the iterative procedure to solve the MCLR equations. Thus either primitive spectra, moments, or the pseudospectra generated from MCLR are used as basic quantities in Stieltjes imaging procedures to obtain the energy-normalized photoionization cross sections. These approaches are evaluated against each other. The MCLR pseudospectrum provides some of spectral moments of the primitive spectrum exactly and some—the higher ones—approximately, but is always possible to compute, while the primitive spectrum may not be. The so-called quadrature spectra can then be obtained from the pseudospectra instead of the primitive spectrum or its moments. This gives an efficient and also a numerically stable procedure for the final continuous oscillator strength distribution.

In the following section we briefly present the MCLR-based approaches for generating photoabsorption-photoionization cross sections. The Stieltjes imaging method is also presented for cases using the spectral moments as primary input. In Sec. IV we present the results for H_2O, HF, and Ne. We compare the three methods employed and investigate the degree of gauge invariance and fulfillment of sum rules, and, furthermore, the dependencies on basis set and reference active space. Finally, in Sec. V, we discuss the formal and numerical aspects of the methods and draw some conclusions from the present investigation.

II. THEORY

A. MCLR approach

Response functions describe how a state, the reference state, reacts to external or internal perturbations. A simple time-dependent response function model is obtained using a self-consistent-field (SCF) state as a reference state. This approach is often referred to as the random-phase approximation and is used as a basic level of theory in the present calculations. Response function methods have also been derived for multiconfiguration self-consistent-field (MCSCF) and coupled-cluster (CC) reference states [20–22] and by using perturbation theory [23]. In the present work we consider response functions where MCSCF states are used as reference states. The MCSCF linear-response functions were derived by Yeager and Jørgensen [20]. In a later formulation Olsen and Jørgensen derived both the linear and quadratic response functions. We use this formulation in the present work. The MCLR approach leads to results that are gauge invariant and sum rules that are fulfilled exactly in the limit of a complete one-electron basis. The spectral representation of the response function is determined by a MCLR two-component eigenvalue equation [17]:

$$\left[\begin{bmatrix} A & B \\ B & A \end{bmatrix} - \omega_n \begin{bmatrix} \Sigma & \Delta \\ -\Delta & -\Sigma \end{bmatrix} \right] \begin{bmatrix} {}^1X_n \\ {}^2X_n \end{bmatrix} = \begin{bmatrix} 0 \\ 0 \end{bmatrix} . \quad (1)$$

A and B are Hessian-type matrices and Σ and Δ are metric-type matrices, which are defined in Eqs. (9)–(12)

in Ref. 24. In short form, Eq. (1) can be written as the generalized eigenvalue equations

$$(\mathbf{E}^{(2)} - \omega_n \mathbf{S}^{(2)})\mathbf{X}_n = 0 \ . \tag{2}$$

An interative solution to Eq. (2) requires that linear transformations are carried out with $\mathbf{E}^{(2)}$ and $\mathbf{S}^{(2)}$ as transformation matrices [24]:

$$\begin{bmatrix} {}^1u \\ {}^2u \end{bmatrix} = \begin{bmatrix} \mathbf{A} & \mathbf{B} \\ \mathbf{B} & \mathbf{A} \end{bmatrix} \begin{bmatrix} {}^1b \\ {}^2b \end{bmatrix}, \quad u = \mathbf{E}^{(2)}\mathbf{b} \ , \tag{3}$$

$$\begin{bmatrix} {}^1m \\ {}^2m \end{bmatrix} = \begin{bmatrix} \mathbf{\Sigma} & \mathbf{\Delta} \\ -\mathbf{\Delta} & -\mathbf{\Sigma} \end{bmatrix} \begin{bmatrix} {}^1b \\ {}^2b \end{bmatrix}, \quad m = \mathbf{S}^{(2)}b \ . \tag{4}$$

An algorithm that determines the few lowest eigenvalues using the linear transformations in Eqs. (3) and (4) was given in Ref. [24]. This algorithm can be viewed as a generalization of the Davidson-Liu algorithm for the symmetric eigenvalue problem and has the same kind of stable convergence. The special feature of the algorithm is that it employs the pairwise structure of the LR eigenvalue equations. The feasibility of our implementation of the MCLR approach lies in the fact that the two matrices $\mathbf{E}^{(2)}$ and $\mathbf{S}^{(2)}$ of large dimensions (10^5–10^6) are never constructed explicitly, and that information about $\mathbf{E}^{(2)}$ and $\mathbf{S}^{(2)}$ is only available through the linear transformations in Eqs. (3) and (4).

The set of transition energies and intensities $\{\omega_n, I_n\}$, which can be obtained from the MCLR eigenvalue equation (1), provides the correct spectrum of excitation energies and intensities in the discrete part of the spectrum, that is, when $\omega_n < E_x^{N-1}$, where E_x^{N-1} is the ionization potential. For $\omega_n > E_x^{N-1}$, each pair of primitive excitation energies and intensity factors forms a discretized representation of the continuum, which, however, does not form a true representation of continuous photoionization cross sections. We employ the Stieltjes imaging technique to extract the correct continuous oscillator strength density from the discretized spectrum. In the Stieltjes imaging procedure the primitive spectrum of Eq. (2) of order N (half-dimension of $\mathbf{E}^{(2)}$) is converted to a quadrature spectrum of order n ($n \ll N$) such that the first $2n$ moments

$$S(-2k) = \sum_{n \ (\neq 0)} \omega_n^{-2k} f_n^{(i)} \ , \tag{5}$$

where

$$f_n^{(i)} = \tfrac{2}{3}|\langle 0|r^{(i)}|n\rangle|^2\omega_n = \tfrac{2}{3}|r_n^{(i)}|^2\omega_n \ , \tag{6}$$

are reproduced. i denotes x, y, or z. This quadrature spectrum is then used to form Stieltjes derivatives for the correctly energy-normalized cross sections. The approach can straightforwardly be used when the dimension of $\mathbf{E}^{(2)}$ is so small that an explicit diagonalization of $\mathbf{E}^{(2)}$ can be carried out. The first $2n$ moments can be determined straightforwardly for large n by summing the individual contributions to the moments. We have previously used this approach in our calculation of the photodetachment cross sections for Li$^-$ [19]. We call this approach the primitive spectrum approach. The Stieltjes imaging techniques connected to the present MCLR ap-

proaches are briefly presented in Sec. II B.

When the dimension of $\mathbf{E}^{(2)}$ is so large that Eq. (2) cannot be diagonalized explicitly we must resort to a different approach for determining the photoionization spectrum. One such approach is to evaluate the spectral moments in Eq. (5) directly without first resorting to the primitive spectrum and then use a Stieltjes imaging technique from that point (a Stieltjes imaging technique for this purpose is outlined in Sec. II B). We refer to this approach, further described in the following, as the direct spectral moment approach. We specifically consider MCSCF linear-response theory [17], where the excitation energies and transition moments are determined by the generalized eigenvalue equation $(\mathbf{E}^{[2]} - \omega_n \mathbf{S}^{[2]})\mathbf{X}_n = 0$ [Eq. (2)] and

$$f_n^{(i)} = \tfrac{2}{3}|r_n^{(i)}|^2\omega_n \ , \tag{7}$$

$$r_n^{(i)} = r^{t(i)}\mathbf{X}_n \ , \tag{8}$$

and the matrices have the paired structure

$$\mathbf{E}^{[2]} = \begin{bmatrix} \mathbf{A} & \mathbf{B} \\ \mathbf{B} & \mathbf{A} \end{bmatrix} \ , \tag{9}$$

$$\mathbf{S}^{[2]} = \begin{bmatrix} S & \mathbf{\Delta} \\ -\mathbf{\Delta} & -\mathbf{S} \end{bmatrix} \ , \tag{10}$$

$$\mathbf{r}^{(i)} = \begin{bmatrix} \mathbf{r}^{(i)} \\ -\mathbf{r}^{(i)} \end{bmatrix} \ . \tag{11}$$

Let us consider the diagonal representation of Eq. (2):

$$\boldsymbol{\epsilon}^{[2]} = \begin{bmatrix} \omega & 0 \\ 0 & \omega \end{bmatrix} = \mathbf{X}'\mathbf{E}^{[2]}\mathbf{X} \ , \tag{12}$$

$$\mathbf{J}^{[2]} = \begin{bmatrix} \mathbf{I} & 0 \\ 0 & -\mathbf{I} \end{bmatrix} = \mathbf{X}^t\mathbf{S}^{[2]}\mathbf{X} \ , \tag{13}$$

$$\boldsymbol{\rho}^{(i)} = \mathbf{X}^t\mathbf{r}^{(i)} \ . \tag{14}$$

The spectral moments in Eq. (5) may be written

$$S^{(i)}(-2k) = \sum_{n \ (\neq 0)} (\omega_n)^{-2k} f_n^{(i)}$$

$$= \tfrac{2}{3} \sum_{n \ (\neq 0)} \langle 0|r_i|n\rangle(\omega_n)^{-2k+2}\omega_n^{-1}\langle n|r_i|0\rangle \ , \tag{15}$$

which, using Eqs. (12)–(14), becomes

$$S^{(i)}(-2k) = \tfrac{2}{3}\rho^{t(i)}(\boldsymbol{\epsilon}^{[2]^{-1}}\mathbf{J}^{[2]})^{2k-2}\boldsymbol{\epsilon}^{[2]^{-1}}\boldsymbol{\rho}^{(i)}$$

$$= \tfrac{2}{3}\mathbf{r}^{(i)}(\mathbf{E}^{[2]^{-1}}\mathbf{S}^{[2]})^{2k-2}\mathbf{E}^{[2]^{-1}}\mathbf{r}^{(i)} \ . \tag{16}$$

The even negative spectral moments can be calculated by successively solving linear-response-type linear equations in the original basis:

$$t^{(i)}_{-2} = \mathbf{E}^{[2]^{-1}}\mathbf{r}^{(i)} \ , \tag{17}$$

$$\mathbf{t}^{(i)}_{-3} = \mathbf{E}^{[2]^{-1}}(\mathbf{S}^{[2]}\mathbf{t}^{(i)}_{-2}) \ , \tag{18}$$

$$\mathbf{t}^{(i)}_{-k} = \mathbf{E}^{[2]^{-1}}(\mathbf{S}^{[2]}\mathbf{t}^{(i)}_{-k+1}) \ , \tag{19}$$

and

$$S(-2k)=(\mathbf{r}^{1,(i)})^t\mathbf{t}^{(i)}_{-2k}, \quad k=1,2,3,\ldots. \tag{20}$$

Note that $(\mathbf{r}^{1,(i)})^t\mathbf{t}^{(i)}_{-2k+1}=0$ because of the paired structure. The odd moments therefore cannot be evaluated in the original basis using this method. The iterative, successive solution of the response type of linear equations makes it possible to treat cases where the dimension of the MCLR equation is so large that the $\mathbf{E}^{[2]}$ and $\mathbf{S}^{[2]}$ matrices cannot be stored, much less diagonalized explicitly. We keep all trial vectors from each successive solution for $\mathbf{t}^{(i)}_j$ [Eqs. (17)–(19)] and we find that if we project Eq. (2) to the subspace of trial vectors and calculate effective spectral moments from this reduced space then the spectral moments of all orders have converged to a given tolerance after having solved explicitly $\mathbf{t}^{(i)}_{-2j}$, $j=1,2,\ldots,m$, m being of low order. In the computations done in this work we found that $m=6$ was sufficient to calculate $S(k)$, $k=-1,-2,\ldots,-15$. $S(0)$ is included in the velocity form but not in the length form; in the latter case we simply set $S(0)$ equal to the total number of electrons (the Thomas-Reiche-Kuhn sum rule).

The direct moment approach requires moments $S(-2k)$ to be evaluated for large k. The spectral moments are solutions to sets of linear equations and it therefore becomes a computationally demanding task to use this approach. Significant savings can be obtained by using the pseudospectrum approach, where accurate representations of higher moments are obtained by solving only the sets of linear equations for lower moments. This accurate representation of higher moments is thus obtained by saving all the trial vectors that are obtained solving for the lower moments and then projecting Eq. (2) to the subspace of these trial vectors. The diagonal representations of this reduced space representation of Eq. (2) may be used as in the primitive spectrum approach to determine spectral moments of high order, summing up individual contributions to the moments.

The spectral moments are thus determined by building up a residual space that spans successive solutions for $\mathbf{t}^{(i)}_j$. The equations for each moment are solved in a reduced basis starting from the trial vectors for all lower moments and generating extra trial vectors using the algorithm of Ref. [24], taking advantage of the paired structure of the trial vectors. After the solutions for the desired number of moments have been determined, the total reduced space can be diagonalized to yield a set of effective states and intensities. We call the projected spectrum obtained the MCLR pseudospectrum which can be used to form the Stieltjes derivatives and then the Stieltjes cross sections. The MCLR pseudospectrum differs from the quadrature spectrum obtained in the conventional Stieltjes imaging procedure (here primitive spectrum approach), which contains excitation energies and intensities $\omega_i^{(n)}$ and strengths $I_i^{(n)}$ that correspond to abscissas and weights of a generalized Gaussian quadrature of order n, and which are made to reproduce the first $2n$ moments exactly (see the next section). In Sec. IV we evaluate the efficiency of the pseudospectrum approach for the calcu-

lation of the photoionization spectrum comparatively with the primitive and the moment spectral approaches.

B. Stieltjes imaging

Among the possible techniques for extracting the continuous oscillator strength density and photoionization cross section from a discretized spectrum, the Stieltjes imaging (SI) moment method has certainly been the most applied, following the work of Langhoff and co-workers [4,5]. The SI approach is based on the hypothesis that an L^2 calculation, although inadequate to describe the structure of the electronic continuum, can nevertheless give converging approximations of the lowest spectral moments. In the present section we describe the SI procedures used in connection with the three MCLR algorithms described in the preceding section.

Starting from the Kramers-Heisenberg expression of the polarizability as a function of a complex frequency z,

$$\alpha(z)=\int_0^\infty \frac{df(\epsilon)}{\epsilon^2-z^2}, \tag{21}$$

where

$$\frac{df(\epsilon)}{d\epsilon}=\sum_i^{\text{discrete}} f_i\delta(\epsilon-\epsilon_i)+g(\epsilon) \tag{22}$$

is the oscillator strength density containing contributions both from the discrete and the continuous electronic spectrum and ϵ is the excitation energy from the ground state, the cross section $\sigma(\omega)$ is proportional to the imaginary part of the polarizability for real values ω of the frequency or, alternatively, to the oscillator strength density in the continuum

$$\sigma(\omega)=\frac{4\pi\omega}{c}\text{Im}[\alpha(\omega)]=\frac{2\pi^2}{c}g(\omega). \tag{23}$$

Equation (21) is particularly convenient for showing that the polarizability is a Stieltjes integral as far as $df(\epsilon)/d\epsilon \geq 0$ in the integration range, which is obviously true for excitations from the ground state. According to the Stieltjes approach, this kind of integral can be convergently approximated, also on the real axis, as

$$\alpha(z)=\int_0^\infty \frac{dF^{(n)}(\epsilon)}{\epsilon^2-z^2}+R_n(z^2), \tag{24}$$

where $F^{(n)}(\epsilon)$ is an approximate cumulative oscillator strength multistep function

$$F^{(n)}(\epsilon)=\begin{cases} 0, & 0<\epsilon<\epsilon_1^{(n)} \\ \sum_{j=1}^l f_j^{(n)}, & \epsilon_l^{(n)}<\epsilon<\epsilon_{l+1}^{(n)} \\ \sum_{j=1}^n f_j^{(n)}, & \epsilon_n^{(n)}<\epsilon \end{cases} \tag{25}$$

given in terms of a quadrature spectrum $\{\epsilon_j^{(n)},f_j^{(n)}\}$ that is defined by the $2n$ equations

$$S(-2k)=\sum_{j=1}^n \frac{f_j^{(n)}}{(\epsilon_j^{(n)})^{2k}}, \quad k=1,2,\ldots,2n. \tag{26}$$

Here the $S(-2k)$ are spectral moments of the true oscillator strength function $f(\epsilon)$:

$$S(-j) = \int_0^\infty \frac{df(\epsilon)}{\epsilon^j} \ . \qquad (27)$$

The convergence properties of expression (25) are such that by differentiating the approximate cumulative function $F^{(n)}(\epsilon)$, an approximate oscillator strength density $dF^{(n)}(\epsilon)/d\epsilon$, which will converge to the correct one upon increasing the order n of the quadrature spectrum, can be obtained. The derivative of $F^{(n)}(\epsilon)$ in the energy continuum $g^{(n)}(\epsilon)$ will be expressed, according to the Stieltjes approach, as

$$g^{(n)}(\epsilon) = \begin{cases} 0, & 0 < \epsilon < \epsilon_1^{(n)} \\ \dfrac{1}{2}\dfrac{f_{i+1}^{(n)} + f_i^{(n)}}{\epsilon_{i+1}^{(n)} - \epsilon_i^{(n)}}, & \epsilon_i^{(n)} < \epsilon < \epsilon_{i+1}^{(n)} \\ 0, & \epsilon_n^{(n)} < \epsilon \ , \end{cases} \qquad (28)$$

which defines, through Eq. (23), a convergent approximation for the cross section. The calculation of $\sigma(\omega)$ is then directly connected to the knowledge of the lowest spectral moments. The moment problem expressed by Eq. (26) can be linearized by a Padé approximant to give the polarizability integral

$$\alpha(z) = \sum_{k=1}^n S(-2k)z^{2(k-1)} + R_n(z^2)$$

$$= \sum_j^n \frac{f_j^{(n)}}{(\epsilon_j^{(n)})^2 - z^2} + R_n(z^2)$$

$$= \frac{P_{n-1}(z^2)}{Q_n(z^2)} + R_n(z^2) \qquad (29)$$

with

$$P_{n-1}(z^2) = \sum_{i=0}^{n-1} a_i^{(n)} z^{2i}, \quad Q_n(z^2) = 1 + \sum_{i=1}^n b_i^{(n)} z^{2i} \ . \qquad (30)$$

The pseudospectrum $\{\epsilon_j^{(n)}, f_j^{(n)}\}$ is then obtained from the roots and residues of the Padé approximant. The coefficients $a_i^{(n)}$ and $b_i^{(n)}$ can be obtained by solving a set of linear equations

$$\sum_{L=1}^n S(-2M + 2L - 2)b_L^{(n)} = -S(-2M - 2) \ ,$$

$$n \le M \le (2n - 1) \ , \qquad (31)$$

$$a_M^{(n)} = \sum_{L=0}^M S(-2M + 2L - 2)b_L^{(n)} \ ,$$

$$0 \le M \le (n - 1) \ , \qquad (32)$$

easily derived from Eq. (29). A nontrivial solution of Eq. (31) can always be found insofar as the $S(-2k)$'s are moments of a nondecreasing distribution, but the numerical implementation of Eqs. (31) and (32) is not convenient if a very large number of moments is employed. In fact, the spectral moments are highly redundant and in order to avoid numerical problems they must be computed with high accuracy. Several suggestions can be found in the

literature for overcoming this problem if the input of the SI algorithm is a "variational" spectrum [25,26]. All the proposed algorithms are essentially based on the use of more stable quantities, instead of the spectral moments, to compute the Padé approximants; nevertheless it can be said that none of these techniques is completely trouble-free if quadrature spectra of high order are computed, and the use of double precision in the computer implementation of the algorithms is highly recommended. For Stieltjes imaging calculations starting from primitive or pseudospectra, we have adopted the approach suggested by Langhoff that is based on a continued fraction approximation of a Stieltjes integral different from the polarizability, so that not only the even, but also the odd negative moments are involved in the Taylor expansion.

The present calculations are all based on the Stieltjes imaging technique, frequently employed and evaluated earlier, and inherit therefore the merits and shortcomings of this technique. The latter refer to finite resolution and the risk of missing sharper (autoionization) resonances which can be smoothed out by the Stieltjes imaging. An example of this is the resonance at 14 eV in the H_2O spectrum which appears in high-resolution experiments. In fact, this finite resolution is connected to the order of the histogram, i.e., the number of spectral moments that can be used with confidence. This in turn is limited by the size of the one-electron basis set. Using a very large basis set and thus a better discretization of the continuum, this resonance feature has been reproduced at the RPA level [12]. We stress the ease of using Stieltjes imaging in connection with the MCLR pseudospectra for quantitative calculations of the shape resonances.

III. COMPUTATION

The prediction of the photoionization cross sections involves several computational steps. We have carried out Hartree-Fock (HF), Møller-Plesset second-order perturbation (MP2), and MCSCF calculations of wave functions, RPA and MCLR calculations for solving the linear response equations to obtain spectral moments, discrete excitation spectra, and pseudospectra, and Stieltjes imaging calculations for the photoionization cross sections. The SIRIUS computer program for wave-function [18] and linear-response [16] calculations has been used. It is interfaced to the STOCOS [27,28] and HERMIT [29] programs for generating integrals over oscillating-type functions and Gaussian-type functions, respectively. Some of the recent updates of the response part of the SIRIUS program used in the present work have also been described in Refs. [30,31]. A preliminary MP2 calculation was performed in order to obtain starting orbitals and physically sound choices of correlating orbital spaces [32]. The division into inactive, active, and secondary orbitals can be rather straightforwardly derived from the MP2 occupation numbers (see Table I) and a posteriori, from the natural occupation numbers obtained from the MCSCF calculations. For H_2O and HF we distinguish two such physically sound choices. In the C_{2v} point group these are given by the complete-active-space (CAS) distribution of eight valence electrons in 4,2,2,0 orbitals, or, respectively, 6,3,3,1, orbitals of a_1, b_2, b_1, a_2 symmetry repre-

TABLE I. MP2 natural occupation numbers for H_2O (>0.001).

Symmetry Orbital	A_1	B_2	B_1	A_2
1	1.9991	1.9650	1.9648	0.0061
2	1.9840	0.0244	0.0217	
3	1.9641	0.0063	0.0057	
4	0.0234	0.0010		
5	0.0118			
6	0.0065			
7	0.0057			
8	0.0009			

sentation (for HF b_2 and b_1 are components of the π orbitals). For neon we have explored the three- and four-shell CASSCF and restricted-active-space SCF (RASSCF) spaces used by Jensen et al. [31] in their calculation of the hyperpolarizability dispersion of neon. Thus the CASSCF space consists of all electron distributions within $2s$, $2p$, $3s$, $3p$, and $3d$ subshells. The three-shell RASSCF contained single and double excitations within these subshells (from $n=2$ to $n=3$ subshells). In the four-shell RASSCF the $n=4$ subshells $4s$, $4p$, $4d$, and $4f$ are added. The core orbitals were kept inactive in all calculations.

Two types of basis sets were chosen. One type consisted of oscillating Slater functions (STOCOS) of the form

$$X_{nlm}(\xi,K,r,\theta,\phi) = A_n(\xi,K)r^{n-1}e^{-\xi r}\cos(Kr)Y_l^m(\theta,\phi)$$

$$(33)$$

containing one-center expanded (OCE) Slater and trigonometric functions [27,6] coupled to angular momentum functions. Such basis sets are known to have double- to triple-ζ quality for ground states of simple hydrides, and have some remarkable properties for the description of electronic continua over a wide range of energies. The basis sets used are practically equivalent to those employed earlier with the static exchange approximation for H_2O [33] and HF [34]. The basis set for the excited orbitals was chosen for a balanced description of the oscillator strength density. Stable results in all regions of spectra are found with a final basis set containing 111 (HF) and 92 (H_2O) s,p,d,f functions, distributed in C_2v symmetry as $52a_1, 24b_2, 24b_1, 11a_2$ and $44a_1, 21b_2, 21b_1, 6a_2$, respectively. High values of nl quantum numbers were included for the adequate description of the electronic cloud localized to the hydrogen atoms. Oscillating functions of s, p, and d symmetries were added on top of the Slater functions, with K parameters ranging from 0.2 to 1.3 and $\Delta K = 0.2$ chosen for the description of the shape resonance region 20 eV above threshold.

The second type of basis set employed consisted of generally contracted approximate-natural-orbital (ANO) Gaussian basis functions [35]. These were augmented with functions with small even-tempered exponents to describe the continuum cross sections. For H_2O we used the 105-CGTO (contracted Gaussian-type orbital) basis set of Müller-Plathe and Diercksen [15]. It

was originally optimized in Ref. [36] to reproduce the Thomas-Reiche-Kuhn (TRK) sum rule at the RPA level, and augmented with more diffuse functions. The suitability of this basis set has already been explored by Müller-Plathe and Diercksen [15] in RPA and second-order polarization propagator calculations of the photoionization cross sections of the water molecule. For HF a systematic basis-set investigation was conducted, testing requirements of both very large and very small orbital exponents and orbital contractions. The requirement is that the basis set should span the ground state with an extended basis set, the excited states, including Rydberg states, and the low-energy continuum. Contracted versus uncontracted core functions were also tried. The first basis set is the one from Lazzaretti et al. [37], which here is left uncontracted. It includes F $14s8p4d$ functions, H $8s3p1d$ functions, and is here augmented with further F ($5s,6p,2d,1f$) and H ($1s$) scaled functions, giving a total of 127 functions. The second Gaussian basis set is a conventional extended basis set (F:$6s,4d,2p$; H:$3s,1p$) augmented with scaled $6s$, $6p$, $6d$, and $4f$ functions (scaling factor 1.8 for s,p,d functions and 3.24 for f functions) giving a total of 136 contracted basis functions. The extra exponents are provided by the authors on request. For HF and H_2O the calculations were carried out at the ground-state equilibrium geometries [$R(OH) = 1.811\,096$ a.u. $\alpha = 104.4499°$; $R(HF) = 1.7328$ a.u.]. For neon we have adopted the basis set of Maroulis and Thakkar [38] that recently has been evaluated for the hyperpolarizability dispersion of neon [39,31].

The order of the histograms used in the Stieltjes imaging were 2–9 for H_2O and HF and 2–6 for Ne. The Stieltjes imaged values were smoothed by using polynomial fitting, giving a variation for different orders of roughly 5%.

IV. RESULTS

In this section we present the RPA and MCLR moment-theory results for the total photoabsorption-photoionization cross sections for water, hydrogen fluoride, and neon. The energy range covered is 0–60 eV, thus including valence-type excitations but excluding excitations of the core electrons. At low energies the photoionization cross sections may differ from the calculated photoabsorption cross sections because of the occurrence of molecular decay channels different from ionization, which reduces the photoionization efficiency. At higher energies, beyond 20 eV, the photoionization efficiency is equal to 1. The dependency of the results on the parametrizations of the theory is explored. The relevant quantities in this respect are the choice of the one-particle and the correlating N-particle (active space) basis sets in the MCLR procedure, the gauge invariance between length and velocity forms for the dipole operator, and the choice between the primitive-, spectral moment-, and pseudospectral forms of the MCLR method. Except for photoionization cross sections, we also present the discrete excitation energies, the Cauchy spectral moments describing zeroth $S(0)$ (Thomas-Reiche-Kuhn sum rule), the second $S(-2)$ (dipole polarizability) moments, and also

higher moments, and compare these with derived experimental moments if available. We also apply the Stieltjes imaging procedure to the moments that have been derived from experimental cross sections in a semiempirical fashion by Meath and co-workers [1,2]. For this we have applied Eqs. (29)–(33) given in Sec. II B. The so reconstructed cross sections provide a test on the internal consistency of the experimental data as well as of the Stieltjes imaging procedure itself.

A. Hydrogen fluoride

The only reported theoretical photoionization cross sections of HF are those of Cacelli *et al.* [12] obtained from single- and multichannel static-exchange-approximation (SEA) and RPA calculations, and by Faegri and Kelly [40] and Hitchcock *et al.* [41] from SEA calculations. Experimental dipole oscillator strengths and cross sections have been given by Salama and Hasted [42], Carnovale and Brion [47], Hitchock and Brion [44], Carnovale, Tseng, and Brion [45], and by Kumar and Meath [2]. The latter put together different sets of experimental data to derive the dipole oscillator strengths distributions and spectral moments.

Figure 1 displays HF absorption cross sections, obtained by applying the Stieltjes imaging procedure to pseudospectra calculated in the RPA, MCLR 422, and MCLR 6331 approximations, compared with the results for experimental cross sections obtained by Brion and Thomson [46]. As for H_2O, we obtain a consistent picture for RPA vs MCLR with an excellent gauge invariance. However, RPA still tends to give somewhat too large cross sections for higher energies. On the other
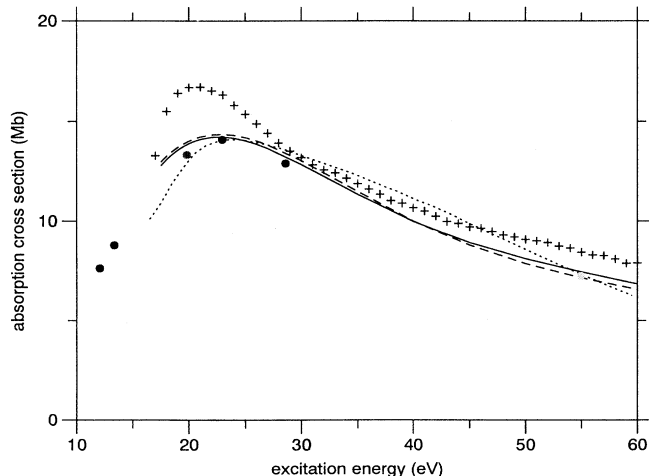
hand, the MCLR 422 and 6331 results are virtually identical, indicating convergence with respect to correlating space already at the 422 level thus fulfilling the rule of thumb of having one correlating unoccupied orbital per strongly occupied valence orbital. Figure 2 shows RPA results for the different basis sets described in Sec. III. Tables II and III show corresponding results for spectral moments with different basis sets and active spaces, and Table IV shows discrete excitation energies and oscillator strengths obtained by RPA, MCLR, and experiment.

As seen by the plots in Fig. 1, the theoretical cross sections for HF at the shape resonance are notoriously too low compared to the data derived by Tseng, Carnovale, and Brion [45] or by Brion and Thomson [46], while at higher energies the computed cross sections are somewhat lower. The deviation is definitely larger than what can be ascribed to the choice of basis set or active space in the MCLR procedure. In this connection we also explored the geometry dependence of the cross sections, but have not found it large enough to sustain a notion of a "vibrationally enhanced" resonance.

Carnovale, Tseng, and Brion [45] used a so-called constant ionic state (CIS) technique from which partial and total oscillator strengths are derived after modification for analyzer transmission and Bethe-Born factors. The relative photoabsorption was placed on an absolute oscillator strength scale by normalizing the total area under the photoabsorption curve to the number of valence electrons using the TRK sum rule (modified by 0.26 for Pauli-principle-forbidden transitions). They then plotted the photoionization efficiency of HF obtained by dividing the sum of CIS partial oscillator strengths by the total photoabsorption oscillator strength. The ionization efficiency was observed to rise at the onsets of the $X\,^2\Pi$ and the $A\,^2\Sigma^+$ channels and flattened out to 1 above 22 eV. However, the efficiency at 21–22 eV was found to be significantly larger than 1 (about 1.1), something which

FIG. 1. HF absorption cross section obtained by applying the Stieltjes imaging procedure to the pseudospectrum calculated in the CAS-6331 approximation (solid line), CAS-422 approximation (dashed line), and in the RPA (dotted line). Big dots indicate values obtained by applying the Stieltjes imaging procedure to the semiempirical negative moments reported by Kumar and Meath [2] while crosses indicate results for experimental cross sections reported by Brion and Thomson [46].

FIG. 2. HF absorption cross section obtained by applying the Stieltjes imaging procedure to the primitive spectrum calculated in the RPA (length gauge) for three different basis sets: STOCOS (solid line), "Gaussian-big" (dashed line), and "Gaussian-laz" (dotted line), explained in Sec. III.

TABLE II. Spectral moments $[S(k)]$ for HF molecule in dipole length and velocity gauges. RPA and MCLR (CAS-422) calculations in length (l) and velocity (v) gauges for z (σ) and y (π_y) moments. Lazzaretti basis set. $S(0)$ "l" entry represents the results for sum rule in mixed representation.

k	RPAzl	RPAzv	RPAyl	RPAyv	MCLRzl	MCLRzv	MCLRyl	MCLRyv
0	9.865	9.837	9.857	9.766	9.858	9.827	9.848	9.752
-1		5.661		4.885		5.835		5.101
-2	5.717	5.710	4.474	4.401	6.149	6.151	5.095	5.006
-3	7.077	7.075	5.377	5.301	7.910	7.926	6.783	6.686
-4	9.843	9.843	7.920	7.828	11.34	11.37	11.09	10.97
-5	14.72	14.72	13.49	13.36	17.41	17.46	20.90	20.74
-6	23.11	23.08	25.43	25.24	27.92	27.98	43.27	43.05
-7	37.46	37.38	51.32	51.00	46.14	46.20	95.30	95.00
-8	62.08	61.90	108.3	107.8	77.85	77.89	218.5	218.1

was related to the uncertainties in the electron transmission function for low-energy electrons [45]. It is therefore not unplausible that the deviation between theory and experiments around the shape resonance at 20–25 eV, which is recovered in all calculations (active spaces and basis sets), can be related to the experimental uncertainties in this energy region. Unfortunately no later HF measurements confirming or disproving the results of Carnovale, Tseng, and Brion [45] have, to our knowledge, been reported, something that probably is related to the difficult handling of this sample.

In order to explore the experimental discrepancy further we computed the cross sections using the semiempirical spectral moments of Kumar and Meath [2]. These authors constructed the final differential oscillator strengths (DOS's) [and the differential oscillator strength distributions (DOSD's)] using several sets of original data covering different energy regions. The original data for the differential dipole oscillator strengths, df/dE, are modified according to constants determined by certain constraints related to the TRK sum rule and to molar refractivity data for the relevant energy interval. In some cases, as for HF [2] (see Sec. IV B) the dipole polarizability $S(-2)$ is also used for the construction of the modified DOS's, the DOSD's, and then the (other) spectral moments $S(k)$. For HF the original cross sections (proportional to df/dE) were taken from Hitchock and Brion

TABLE III. Spectral σ (z) moments $[S(k)]$ for HF with different basis sets and active spaces. A: RPA calculations with Lazzaretti basis set. Velocity form. B: RPA calculations with "big" basis set. Velocity form. C: MCLR-4220 calculations with Lazzaretti basis set. Velocity form. D: MCLR-6331 calculations with "big" basis set. Velocity form.

k	A	B	C	D
0	9.837	8.793	9.827	8.699
-1	5.661	5.710	5.835	5.795
-2	5.710	5.766	6.151	6.104
-3	7.075	7.140	7.926	7.886
-4	9.843	9.926	11.37	11.37
-5	14.72	14.82	17.46	17.55
-6	23.08	23.21	27.98	28.27
-7	37.38	37.52	46.20	46.89
-8	61.90	62.04	77.89	79.39

[44], Carnovale and Brion [47], and Salama and Hasted [42]. The results for the negative moments are given in Table III together with the RPA and MCLR data. The final Stieltjes imaging values for the cross sections using the S_k values constructed by Kumar and Meath [2] are given in Fig. 1 as circles. Results are presented for different numbers of moments used (6, 8, or 10). As for neon (see Sec. IV C), the obtained cross sections are in excellent agreement with MCLR computed cross sections, regardless of the number of moments actually used. Considering this agreement between theory and results from modified experimental moments, the excellent gauge invariance, convergence of computational parameters (basis set), choice of correlating method, viz., RPA (no correlation), SOPPA (Sec. IV B), MCLR-CAS, and MCLR-RAS (see also Sec. II C), we are confident that the theory can distinguish between the experimental results for HF and also other molecules of similar size (see further discussion on H_2O and neon data in Secs. IV B and IV C).

One should in this context stress the good values of dipole polarizability and the gauge invariance obtained [$5.45a_0^3$ (length) and $5.39a_0^3$ (velocity)] to be compared with, for instance, the pseudo-natural-orbital configuration-interaction (PNCO-CI) value of $5.50a_0^3$ of Werner and Meyer [48], and an interpolated value of $5.601a_0^3$ given by Kumar and Meath [2]. The good polarizability is consistent with a good description of the photoionization cross sections at low energies, since with small energies (ω's) and large oscillator strength distributions ($df/d\omega$) the cross-section spectrum gives particularly large contributions to the polarizability (note $\alpha = S(-2) \propto \int_{E_0}^{\infty} [df(\omega)/\omega^2]$). The shape resonance region is, however, not so sensitive to the fulfillment of the TRK sum rule, since this involves excitations to high energies.

The agreement obtained for the MCLR photoionization cross sections with the data derived by Kumar and Meath [2] is gratifying also from the point of view that the dipole oscillator strength distribution and spectral moments $S(k)$ relate to a number of other important properties for a molecule, i.e., the straggling ($k = -1$), stopping ($k = 0$), and total ($k = 1$) inelastic cross sections of fast charged particles, dipole polarizabilities ($k = -2$), charge densities at the nuclei ($k = 2$), static and frequency-dependent polarizabilities

TABLE IV. Vertical singlet excitations for HF.

Symmetry	ω_{RPA}	f^l_{RPA} [a]	f^v_{RPA} [a]	ω_{MCLR}	t^l_{MCLR} [a]	f^v_{MCLR} [a]	ω_{expt} [b]
¹Σ-¹Σ⁺	14.85	0.0407	0.0410	13.76	0.0030	0.0029	15.21
	15.66	0.1204	0.1215	14.85	0.0070	0.0069	15.35
	16.15	0.0130	0.0129	14.99	0.0733	0.0724	16.47
	16.48	0.0103	0.0105	15.33	0.0756	0.0755	
	16.84	0.0054	0.0056	15.54	0.0076	0.0799	
	16.96	0.0021	0.0022	15.69	0.0112	0.0113	
	17.22	0.0081	0.0085	15.93	0.0146	0.0152	
	17.30	0.0005	0.0005	16.02	0.0005	0.0005	
¹Σ-¹Π	11.67	0.0321	0.0320	10.90	0.0391	0.0391	10.35
	14.54	0.023	0.0320	13.47	0.0174	0.0172	13.03
	15.53	0.0009	0.0009	14.30	0.0011	0.0011	13.91
	16.12	0.0089	0.0088	14.83	0.0009	0.0009	14.57
	16.20	0.0000	0.0000	14.91	0.0067	0.0067	15.52
	16.21	0.0055	0.0055	15.05	0.0037	0.0036	16.20
	16.28	0.0037	0.0036	15.52	0.0003	0.0003	
	16.59	0.0002	0.0002	15.31	0.0043	0.0041	

[a]The oscillator strengths are given for one component of the degenerate Π excitations.

[b]Experimental 0-0 energies from Hitchcock and Brion [44] and Douglas and Greening [49]. The assignment of experimental transitions to the symmetries follows Cacelli, Carravetta, and Moccia [33].

$(k = -2, -4, -6, \ldots)$, and dispersion energies $(k = -1, -3, \ldots)$. The efficient evaluation of the spectral moments by means of the techniques described in Sec. II A can thus provide important means for calculations of such properties.

B. Water molecule

Most previous theoretical calculations of photoionization cross sections for water have been carried out in the static-exchange and the random-phase approximations; see, e.g., Refs. [34,12] and references therein. The focus in these studies have mostly been on the partial photoionization cross sections, where the coupling between different ionization channels (defined by the molecular orbitals ionized) is neglected. However, multichannel calculations (MCSEA, MCRPA) have also been carried out in order to explore the effects of channel coupling on the total cross sections [12]. In the recent study of Müller-Plathe and Diercksen [15] the RPA calculations were augmented with calculations employing the second-order polarization propagator methods in order to explore the role of correlation on the partial and total cross sections.

Many experimental investigations of the photoionization cross sections of water have been conducted; see e.g., results from Tan et al. [50], Brion and Thomson [46], Katayama, Huffman, and O'Bryan [51], Reilhac and Damany [52], and Haddad and Samson [53]. The various experimental results are reproduced in Fig. 3. Note the deviation between the experiments in the region between 20 and 30 eV, where the most recently presented cross sections, the ones by Haddad and Samson [53], are significantly larger than those given earlier. The solid line in Fig. 3, reproducing the present pseudospectral results from the 422 MCLR calculations, clearly agrees best with the cross sections by Tan et al. [50] and Brion and Thomson [46], while for larger energies the best

agreement is with the data of Reilhac and Damany [52]. For small excitation energies the comparison between computed photoabsorption cross sections and measured photoionization cross sections is hampered by the fact that not all molecular decay channels lead to ionization. However, beyond approximately 20 eV the photoionization efficiency is close to 100%.

Repeating the calculations giving the results of Fig. 3, but using the velocity gauge of the dipole operator, we obtain practically the same results. The gauge invariance
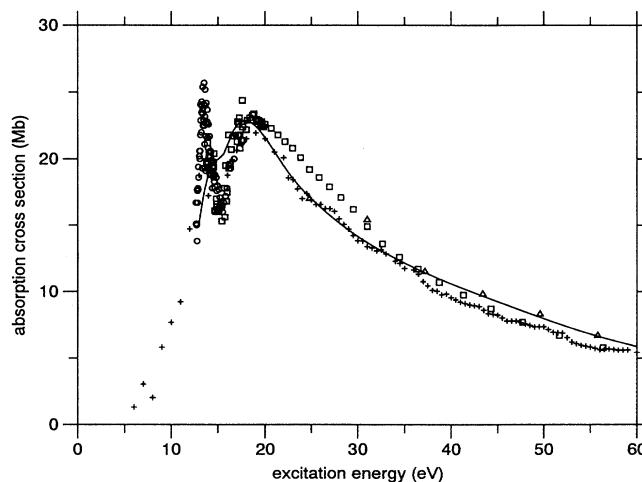
FIG. 3. H_2O absorption cross section (solid line) obtained by applying the Stieltjes imaging procedure to the pseudospectrum calculated in the CAS-422 approximation (length gauge). Experimental results are indicated by crosses (Tan et al. [50] and Brion and Thomson [46]), circles (Katayama, Huffman, and O'Bryan [51]), triangles (Reilhac and Damany [52]), and squares (Haddad and Samson [53]).

is excellent, the deviation being 1% or 2%, to be compared with the experimental uncertainty of some 10%. This observation is confirmed by Tables V and VI, which present dipole length and velocity results for oscillator strengths of discrete excitations and for spectral moments, respectively. The results from corresponding RPA calculations are given by Figs. 4 (length) and 5 (velocity). We see that the gauge invariance of the cross sections are excellent despite the fact that some variations in the primitive spectrum can be noted, at least for higher energies. The gauge invariance in RPA is good, although somewhat poorer than in the MCLR case. It should be pointed out that with the linear-response theory employed the gauge invariance refers to the completeness of the one-electron basis set and not to the level of correlation as such. Comparing the absolute cross sections, the RPA calculations give larger cross sections in the full energy range, with a satisfying overall experimental agreement, although less good than in the MCLR case. Thus our MCLR results improve the RPA results, but the latter compares better with the experimental results of Haddad and Samson [53] in the 20–30 eV range.

The SOPPA results of Müller-Plathe and Diercksen give lower cross sections than the RPA results. The worse agreement between SOPPA results with respect to the more recent experiment of Haddad and Samson [53] in the 20–30-eV region was explained as being due to an overestimation of the $1b_2$ orbital cross section and was traced to a shortcoming in the SOPPA approximation. However, the present MCLR results reinforce the SOPPA results, insofar as a very good agreement with the experiment of Tan et al. [50] is obtained. In the comparison with experimental results one has to bear in mind the uncertainty of published dipole oscillator strength data, with typical errors between 5% and 20% [2]. This seems to be confirmed by the present investigation on H_2O, and also for HF and Ne.

In an attempt to distinguish between the experimental data we have used experimental moments Zeiss et al. [1] derived in the same manner as in Ref. [2] for HF. Unfortunately, the lack of higher moments made it impossible to cover all the relevant parts of the spectrum in the same manner as for the HF spectrum. The Stieltjes imaged cross sections were obtained as 20 Mb at 14 eV and 22 Mb at 18 eV.

H_2O absorption cross sections obtained by applying the
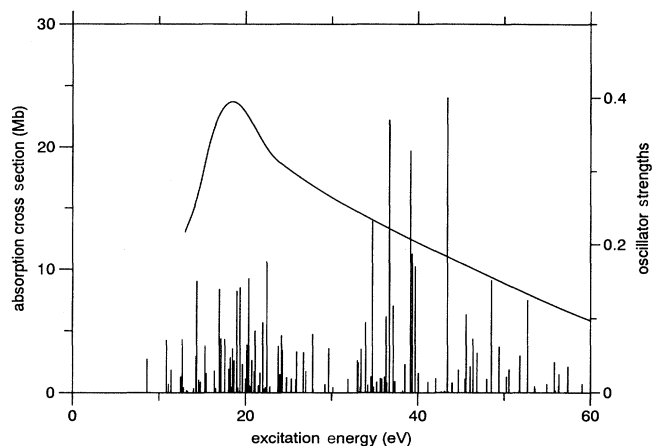
FIG. 4. H_2O absorption cross section (solid line) obtained by applying the Stieltjes imaging procedure to the pseudospectrum (bar diagram) calculated in the RPA approximation (length gauge).

Stieltjes imaging procedure to the primitive spectrum (primitive spectrum approach) gives, in both velocity and length gauges, results virtually identical to those obtained by the pseudospectral approach. Figure 6 collects the results for the absorption cross sections (RPA approximation, length gauge) for water obtained by applying primitive and pseudospectral approaches and also those obtained from moments (direct spectral moment approach). It is clear that the best shape of the photoionization curve is obtained by primitive and pseudospectral results, while a deviation can be noticed for the moment-generated cross sections. It is clear from our investigation that the moment method is more demanding from the numerical point of view, requiring rather many moments to be given with high precision. Because the pseudospectrum is obtained from the MCLR calculations with basically the same effort (see Sec. II A), this procedure is preferable.

C. Neon atom

Being isoelectronic with H_2O and HF, the neon atom fulfills the same zeroth-order (TRK) sum rule for the integrated photoexcitation-photoionization cross sections.

TABLE V. Spectral moments $[S(k)]$ for H_2O molecule. R denotes RPA, M denotes MCLR calculations with 4220 active space and with basis set described in Sec. III.

k	$R A_1 v$	$M A_1 l$	$M A_1 v$	$R B_2 v$	$M B_2 l$	$M B_2 v$	$R B_1 v$	$M B_1 l$	$M B_1 v$
0	9.756		9.738	9.795		9.776	9.646		9.629
−1	6.950		7.185	7.406		7.564	6.429		6.758
−2	8.433	9.374	9.322	9.119	9.753	9.682	7.731	9.277	9.060
−3	12.88	15.48	15.43	13.22	14.72	14.64	12.75	17.46	17.15
−4	22.98	29.93	29.84	21.07	24.46	24.35	26.51	41.70	41.09
−5	45.61	64.27	64.01	35.67	43.30	43.12	64.70	116.0	114.5
−6	97.41	147.7	147.0	62.99	80.25	79.89	174.9	353.9	349.5
−7	218.4	355.3	353.3	114.7	154.1	153.4	503.1	1139.	1125.
−8	506.3	879.9	874.5	213.8	305.2	303.6	1501.	3782.	3739.
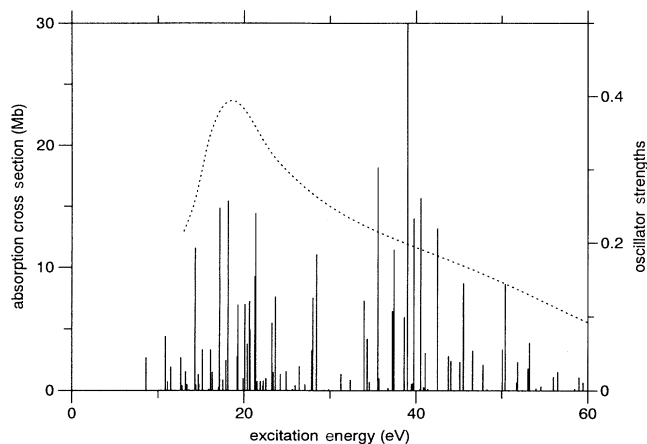
FIG. 5. Same as Fig. 4 but with the velocity gauge (dashed line).

Thus the order of the cross sections relating as $\sum$ (Ne) $< \sum(F) < \sum(O)$ at low energies is reversed at higher energies. The maximum of the cross section is also shifted to lower energies along this sequence. These trends, followed also by N (NH$_3$) and C (CH$_4$), have been rationalized by Debies and Rabalais [56] in terms of the number of hydrogen atomic orbitals in the molecules and the radial extent of the $2s$ and $2p$ orbitals, which increases as the atomic number decreases from Ne to C.
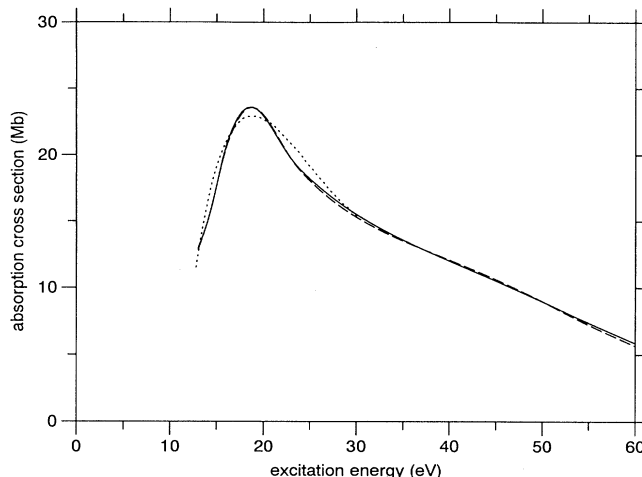
FIG. 6. H$_2$O absorption cross section obtained by applying the Stieltjes imaging procedure to the primitive spectrum (solid line), to the pseudospectrum (dashed line) and to the even negative moments (dotted line) calculated in the RPA approximation (length gauge).

Figure 7 compares results for the Stieltjes imaged Ne absorption cross sections obtained from the pseudospectrum calculated in the MCLR-CAS, MCLR-RAS, and RPA approximations. We find the CAS and RAS results to be virtually identical. For higher energies they coin-

TABLE VI. Vertical singlet excitations for H$_2$O.

Symmetry	ω_{RPA}	f^l_{RPA}	f^v_{RPA}	ω_{MCLR}	f^l_{MCLR}	f^v_{MCLR}	ω_{expt} [a]
$^1A_1$-$^1B_1$	8.61	0.0455	0.0449	7.81	0.0530	0.0524	7.440
	11.11	0.0118	0.0117	10.07	0.008 3	0.008 2	9.998
	11.85	0.0000	0.0000	10.72	0.000 1	0.000 1	10.640
	12.51	0.0202	0.0201	11.29	0.024 2	0.023 9	10.990
	12.66	0.0139	0.0137	11.47	0.018 8	0.018 4	11.122
	12.86	0.0074	0.0070	11.71	0.008 1	0.007 8	11.374
	13.20	0.0032	0.0031	12.25	0.000 8	0.001 0	
	13.30	0.0022	0.0024	12.40	0.001 8	0.001 7	
$^1A_1$-$^1A_1$	10.86	0.0711	0.0706	10.04	0.023 6	0.023 3	9.850
	11.40	0.0309	0.0309	10.43	0.079 2	0.079 0	10.171
	12.72	0.0220	0.0216	11.52	0.026 3	0.025 8	11.057
	13.24	0.0000	0.0000	12.35	0.000 01	0.000 01	11.432
	13.62	0.0009	0.0009	12.63	0.000 1	0.000 1	12.9
	14.01	0.0060	0.0060	13.11	0.008 5	0.008 4	
	14.48	0.0177	0.0173	13.61	0.020 7	0.020 3	
	14.75	0.0110	0.0109	13.80	0.013 3	0.013 2	
$^1A_1$-$^1B_2$	12.51	0.0018	0.0018	11.39	0.022 7	0.022 4	11.041
	12.70	0.0500	0.0498	11.96	0.025 5	0.025 4	13.8
	14.27	0.1513	0.1509	13.42	0.046 2	0.046 4	16.9
	14.34	0.0000	0.0000	14.25	0.034 2	0.034 5	
	15.05	0.0189	0.0181	14.49	0.138 2	0.137 0	
	16.39	0.0004	0.0004	15.43	0.001 2	0.001 5	
	16.87	0.1398	0.1411	15.77	0.205 3	0.205 0	
	16.95	0.0721	0.0718	17.01	0.0223 1	0.022 4	

[a]From Ref. [54]; see also Ref. [55]. The assignment of experimental transitions to the symmetries follows Cacelli, Carravetta, and Moccia [34].
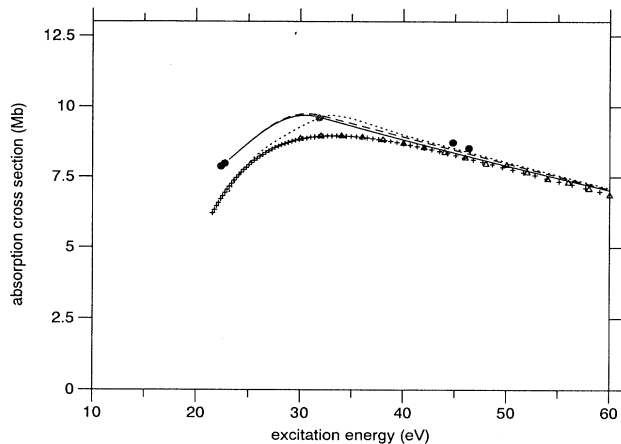
FIG. 7. Neon absorption cross section obtained by applying the Stieltjes imaging procedure to the pseudospectrum calculated in the CAS (solid line), RAS (dashed line), and in the RPA (dotted line) approximations. Big dots indicate values obtained by applying the Stieltjes imaging procedure to the semiempirical negative moments reported by Kumar and Meath [2], while circles and crosses indicate experimental results by Marr and West [57] and Wuilleumier and Krause [58], respectively.

cide with RPA results, while for the energy region with enhanced cross sections between 30 and 40 eV there is a difference; RPA pushes the cross section peak to higher energies. For neon we adopted one sole basis set [38], the one that recently was evaluated for the hyperpolarizability dispersion of neon [39,31]. Figure 7 also includes experimental results by Marr and West [57] and Wuilleumier and Krause [58]. The data given by the latter authors constitute an averaged compilation of four different experimental tabulations [59,60,61,57]. An uncertainty between 4–8 % was estimated for the total cross sections obtained this way. It can also be noted that the error bars for the partial cross sections derived from the averaging procedure were largest at the position of the shape resonance, where the experimental-to-theoretical deviation is at its largest. Above 50 eV the sets of experimental and theoretical data agree well, mutually and internally. In order to check the possible origin of the deviation we applied the Stieltjes imaging procedure to the semiempirical negative moments reported by Kumar and Meath [2] obtained by imposing similar constraints as in the cases of H_2O and HF (see previous sections).

Results are shown in Fig. 7 for cross sections obtained with 6, 8, and 10 spectral moments. Again we can notice an excellent agreement between cross sections obtained this way and those obtained from MCLR (CAS, RAS) pseudospectral data. Table VII shows the spectral moments for neon obtained by various methods.

V. DISCUSSION AND CONCLUSIONS

We have presented multiconfigurational linear-response theory for photoionization and photodetachment cross sections in atoms and molecules. From the solutions of the MCLR equations the primitive spectrum of excitation energies and oscillator strengths are obtained. We have shown that these solutions can be used to provide the even negative moments of the photoexcitation-photoionization spectrum. We have also shown that the pseudospectrum can be constructed directly in the iterative procedure to solve the MCLR equations. Either the primitive spectra, the moments, or the pseudospectra are used as basic quantities in Stieltjes imaging to obtain the energy-normalized photoionization cross sections.

From the numerical point of view the use of MCLR pseudospectra gives close to identical results as the procedure based on the MCLR primitive spectrum. The use of (MCLR-generated) spectral moments are, however, found somewhat inferior in this respect. We find for H_2O, HF, and Ne that the inclusion of electron correlation is significant but also that small correlating spaces seems to be sufficient. The choice of a one-particle basis set is more crucial; however, for the type of systems studied here, convergence with respect to the basis set can easily be achieved. Successive enlargement of the correlating space can also easily be accomplished, e.g., by using criteria from perturbation theory. In general we find excellent agreement between the dipole length and dipole velocity gauges using RPA and MCLR. A good agreement of the second-order sum rule, the polarizability, is a prerequisite for a good representation of the cross sections at the low-energy resonant region, while the fulfillment of the TRK sum rule requires a more balanced description of the whole spectrum, also including core excitations into the high-energy continuum. Higher negative spectral moments become progressively more important for determining the low-energy cross sections correctly.

With RPA- or MCLR-generated spectra a separate channel interpretation is not possible to obtain since the different orbital excitations are mixed, and there is no

TABLE VII. Spectral moments $[S(k)]$ for neon atom from Ref. [31].

k	CAS	3-shell	RAS 3-shell	RAS 4-shell	Estimate	Expt.[a]
-2	2.598	2.564	2.594		2.642 ± 0.049	2.669
-3	2.397	2.340	2.388		2.471 ± 0.081	2.533
-4	2.634	2.567	2.618		2.711 ± 0.093	2.886
-5	3.239	3.099	3.210		3.406 ± 0.196	3.686

[a]Reference [62].

unique way to identify the cross sections for the individual channels. On the other hand, this means that one avoids the artificial discontinuities at the ionization potentials that the separate-channel approximation may cause by summing up cross sections from the independent channels. Experimentally, such discontinuities are not observed since channel coupling smooths the cross sections in the vicinity of the ionization potentials. The effect of the inclusion of channel interaction is significant for the total cross sections in the shape resonance region around 20 eV of the presently investigated species. For example, in the water cross-section spectrum, this turns up in the determination of the partial cross sections for the $1b_2$ orbital channel [12,15].

A problem in common moment-theory calculations is the occurrence of discrete states embedded in the continuum. The presence of such states leads to discrete-continuum interactions that may alter the total cross sections in the relevant energy regions. The effects of this type of interaction have also been treated by Stieltjes imaging procedure but using the δ energy interaction of the Hamiltonian instead for constructing the basic discrete-continuum interactions [12]. The occurrence of quasi-discrete states may also lead to a discrepancy between absorption cross sections and ionizations cross sections [63], due to fluorescence decay or dissociation of these discrete states. Here rules of thumb are used to determine if these states are included or not. For RPA the relevant ionization potentials are given by Koopman's theorem, while MCLR intrinsically includes relaxation. In the multiconfigurational linear-response approach, the channels are coupled by the choice of correlating orbital space (active space). The occurrence of an interaction with quasidiscrete states (autoionization) is accounted for insofar as it can be described as excitations within the or-

bital space encompassed by the ground-state active space. In practice, the active space is chosen by the correlation contributions to the ground state (natural occupation numbers), and it is difficult to know *a priori* if the appropriate orbitals are included or not.

The use of MCLR makes it possible to go beyond the static exchange approximation based on the strong orthogonality condition for the photoelectron. The photoionization dynamics described by the correlation of all electrons (polarization of the residual ion) including the photoelectron is therefore accounted for in principle. This is particularly important for low-lying resonances and cross sections close to threshold. Practically, the calculations of the cross sections at low energies will still be difficult since these require exceedingly rich basis-set representations of the primitive spectrum just above threshold in order to obtain stable cross sections in this region. MCLR, like previously employed RPA, SOPPA, and MCRPA, fulfills sum rules and is gauge invariant in the limit of a complete basis set. These propagator-oriented approaches are thus more attractive than the static exchange approaches in this respect. The use of MCLR means that the body of photoionization resonance calculations can be enlarged to encompass difficult and exotic cases. It includes general open-shell states with unusual electronic structures with strongly correlated wave functions. In particular, it can address molecular anions for which a good correlated treatment of the ground-state wave functions is a necessity. The photodetachment of these species will be the subject of forthcoming studies.

[1] G. D. Zeiss, W. J. Meath, J. C. F. MacDonald, and D. J. Dawson, Can. J. Phys. **55**, 2080 (1977).

[2] A. Kumar and W. J. Meath, Can. J. Chem. **63**, 1616 (1985).

[3] A. M. Bradshaw and J. Sommers, Phys. Scr. **T31**, 189 (1990).

[4] P. W. Langhoff, in *Electron Molecule and Photon Molecule Collisions,* edited by T. N. Rescigno, B. V. McKoy, and B. Schneider (Plenum, New York, 1979), p. 183.

[5] P. W. Langhoff, in *Theory and Application of Moment Methods in Many-Fermion Systems,* edited by B. J. Dalton, S. M. Grimes, J. P. Vary, and S. A. Williams (Plenum, New York, 1980), p. 191.

[6] I. Cacelli, V. Carravetta, A. Rizzo, and R. Moccia, Phys. Rep. **205**, 283 (1991).

[7] I. Cacelli, V. Carravetta, and R. Moccia, J. Chem. Phys. **85**, 7038 (1986).

[8] T. N. Rescigno and C. W. McCurdy, Phys. Rev. A **31**, 624 (1985).

[9] R. M. Pitzer and C. W. McCurdy, Phys. Rev. A **32**, 213 (1985).

[10] W. J. Hunt and W. A. Goddard III, Chem. Phys. Lett. **3**, 414 (1969).

[11] K. Kaufmann, W. Baumeister, and M. Jungen, J. Phys. B

20, 4299 (1987).

[12] I. Cacelli, V. Carravetta, R. Moccia, and A. Rizzo, J. Phys. Chem. **92**, 979 (1988).

[13] I. Cacelli, V. Carravetta, and R. Moccia, Chem. Phys. **120**, 51 (1988).

[14] P. Swantstrøm, J. T. Golab, D. L. Yeager, and J. A. Nichols, Chem. Phys. **110**, 339 (1986).

[15] F. Müller-Plathe and G. H. Diercksen, Phys. Rev. A **40**, 696 (1989).

[16] H. J. Aa. Jensen, J. Olsen, and P. Jørgensen, J. Comp. Chem. **74**, 265 (1988).

[17] J. Olsen and P. Jørgensen, J. Chem. Phys. **82**, 3235 (1985).

[18] H. J. Aa. Jensen, H. Ågren, and J. Olsen, *Molecular Techniques in Computational Chemistry,* edited by Enrico Clementi (Escom, Leiden, 1990).

[19] V. Carravetta, H. Ågren, P. Jørgensen, and J. Olsen, J. Phys. B **22**, 2133 (1989).

[20] D. L. Yeager and P. Jørgensen, Chem. Phys. Lett. **65**, 77 (1979).

[21] E. Dalgaard, J. Chem. Phys. **72**, 816 (1980).

[22] E. Dalgaard and H. J. Monkhorst, Phys. Rev. A **28**, 1217 (1983).

[23] J. Oddershede and P. Jørgensen, J. Chem. Phys. **66**, 1541 (1977).

[24] J. Olsen, H. J. Aa. Jensen, and P. Jørgensen, J. Comput. Phys. **74**, 265 (1988).

[25] P. W. Langhoff, C. T. Corcoran, J. S. Sims, and F. Weinhold, Phys. Rev. A **14**, 1042 (1976).

[26] R. K. Nesbet, Phys. Rev. A **14**, 1065 (1976).

[27] V. Carravetta and I. Cacelli, IBM Research Report No. KGN196, 1989 (unpublished).

[28] I. Cacelli, V. Carravetta, A. Rizzo, and R. Moccia, in *Modern Techniques in Computational Chemistry* (Ref. [18]), p. 639.

[29] T. U. Helgaker and P. R. Taylor (unpublished).

[30] P. W. Fowler, P. Jørgensen, and J. Olsen, J. Chem. Phys. **82**, 3235 (1990).

[31] H. Hettema, H. J. Aa. Jensen, P. Jørgensen, and J. Olsen, J. Chem. Phys. **97**, 1174 (1992).

[32] H. J. Aa. Jensen, P. Jørgensen, H. Ågren, and J. Olsen, J. Chem. Phys. **88**, 3834 (1988).

[33] I. Cacelli, V. Carravetta, and R. Moccia, J. Phys. B **18**, 1375 (1985).

[34] I. Cacelli, V. Carravetta, and R. Moccia, Chem. Phys. **90**, 313 (1984).

[35] P.-O. Widmark, P. Å. Malmquist, and B. O. Roos, Theor. Chim. Acta **77**, 291 (1990).

[36] P. Lazzaretti and R. Zanasi, J. Chem. Phys. **83**, 1218 (1985).

[37] P. Lazzaretti, E. Rossi, and R. Zanasi, Phys. Rev. A **27**, 1301 (1983).

[38] G. Maroulis and A. J. Thakkar, Chem. Phys. Lett. **156**, 187 (1989).

[39] P. R. Taylor, T. J. Lee, J. E. Rice, and J. Almlöf, Chem. Phys. Lett. **163**, 359 (1989).

[40] K. Faegri and H. P. Kelly, Phys. Rev. A **23**, 52 (1981).

[41] H. P. Hitchcock, Q. R. J. Williams, C. E. Brion, and P. W. Langhoff, Chem. Phys. **88**, 64 (1984).

[42] A. Salama and J. B. Hasted, J. Phys. B **9**, L333 (1976).

[43] I. Cacelli, V. Carravetta, and R. Moccia, J. Phys. B **16**, 1895 (1983).

[44] A. P. Hitchcock and C. E. Brion, Chem. Phys. **61**, 281 (1981).

[45] F. Carnovale, R. Tseng, and C. E. Brion, J. Phys. B **14**, 4771 (1981).

[46] C. E. Brion and J. P. Thomson, J. Electron Spectrosc. Relat. Phenom. **33**, 301 (1984).

[47] F. Carnovale and C. E. Brion, Chem. Phys. **74**, 253 (1983).

[48] H. J. Werner and W. Meyer, Mol. Phys. **31**, 855 (1976).

[49] A. E. Douglas and F. R. Greening, Can. J. Phys. **57**, 1650 (1979).

[50] K. H. Tan, C. E. Brion, Ph. E. van der Leeuw, and M. J. van der Wiel, Chem. Phys. **29**, 299 (1978).

[51] D. H. Katayama, R. E. Huffman, and C. L. O'Bryan, J. Chem. Phys. **59**, 4309 (1973).

[52] L. de Reilhac and N. Damany, J. Quant. Spectrosc. Radiat. Transfer **18**, 121 (1977).

[53] G. N. Haddad and J. A. R. Samson, J. Chem. Phys. **84**, 6623 (1986).

[54] P. Gütler, V. Saile, and E. E. Koch, Chem. Phys. Lett. **51**, 386 (1977).

[55] H. T. Wand, W. S. Felps, and S. P. McGlynn, J. Chem. Phys. **67**, 2614 (1977).

[56] T. P. Debies and J. W. Rabalais, J. Am. Chem. Soc. **97**, 487 (1975).

[57] G. V. Marr and J. B. West, At. Data Nucl. Data Tables **18**, 497 (1976).

[58] F. Wuilleumier and M. O. Krause, J. Electron. Spectrosc. Relat. Phenom. **15**, 15 (1979).

[59] B. L. Henke and R. L. Elgin, Adv. X-Ray Anal. **13**, 639 (1970).

[60] W. S. Watson, J. Phys. B **5**, 2292 (1972).

[61] J. A. R. Samson, private communication in J. Electron. Spectrosc. **15**, 15 (1979).

[62] D. M. Bishop, Phys. Rev. Lett. **65**, 1688 (1990).

[63] R. H. Page, R. J. Larkin, Y. R. Shen, and Y. T. Lee, J. Chem. Phys. **84**, 6623 (1988).